ISBN: 978-3-95450-236-3 ISSN: 2673-5350 doi:10.18429/JACoW-IBIC2023-TH2C03

ANALYSIS OF THE TRANSVERSE SCHOTTKY SIGNALS IN THE LHC

K. Lasocha*, D. Alves, CERN, Geneva, Switzerland

Abstract

Schottky-based diagnostics are remarkably useful tools for the non-invasive monitoring of hadron beam and machine characteristics such as the betatron tune and the chromaticity. In this contribution recent developments in the analysis of the transverse Schottky signals measured at the Large Hadron Collider will be reported. A fitting-based technique, where the measured spectra are iteratively compared with theoretical predictions, will be presented and benchmarked with respect to the previously known methods and alternative diagnostic.

INTRODUCTION

Schottky signals are the fluctuations of macroscopic beam characteristics, such as intensity or dipole moment, due to the discrete nature of the particle ensemble. They were first measured at the CERN's Intersecting Storage Ring in the early 1970s [1] and immediately used to provide information on momentum spread and betatron tune, as well as the rate of growth of betatron amplitudes at tune values close to resonant lines. Notably, it was the observation of Schottky signals what convinced Simon van der Meer to persue the implementation of his eminent concept of stochastic cooling [2].

Since then, the Schottky signal analysis has become a standard diagnostic technique for both coasting and bunched hadron beams, used among others in Tevatron [3], RHIC [4], SIS18 [5], CSR [6], ELENA [7] and LHC [8]. The basic theory of Schottky signals of coasting beams [9] has been enriched by studies on the Schottky spectrum deformation due to space charge, impedance and collective effects present in dense cooled beams [10, 11].

The case of Schottky signals of bunched beams is much less understood. The theory describing such signals is more complex, as it also has to take into account the particles' synchrotron motion. Some main principles can be found in Refs. [12, 13], as well as the effect of space-charge [14], but the knowledge on the impact of impedance, octupole magnets or beam-beam effects on Schottky spectra is so far very limited.

In addition, bunching introduces a finite degree of correlation in the motion of individual particles. In steady-state conditions, thanks to the filamentation associated with the betatron and synchrotron motion of particles, this correlation (also known as coherent motion) has a limited impact on the observed Schottky spectrum. Nevertheless, in certain conditions coherent effects are not negligible, yet very difficult to describe quantitatively.

* kacper.lasocha@cern.ch

In this contribution we shall recall the theory of the transverse Schottky spectra of bunched beams. Using experimental Schottky spectra measured during the ongoing LHC Run3 (2022-2026), we will address the issues of how and when the theory can be used to derive parameters such as the betatron tune and chromaticity. We shall also apply a fitting-based technique, proposed in [15, 16], which can be used to derive transverse beam characteristics from the spectrum, even in the presence of coherent components.

THEORY

Let us consider first the Power Spectral Density (PSD) of a transverse Schottky signal originating from a single particle. Around every harmonic h of the revolution frequency ω_0, the PSD consists of two bands, described by the following expression

$$P_T^{\pm}(\omega, \widehat{\tau}, \Omega_{s_0}, Q, Q\xi) =$$

$$= \hat{a} \sum_{p=-\infty}^{\infty} J_p^2 \left(\chi^{\pm}_{\widehat{\tau}, h\mp Q_I} \right) \delta[\omega - (h \pm Q_F)\omega_0 - p\Omega_s(\widehat{\tau})], \quad (1)$$

where Q_I and Q_F denote respectively the integer and fractional part of the betatron tune Q, $Q\xi$ is the chromaticity, $\widehat{\tau}$ is the time amplitude of synchrotron motion, $\Omega_s(\widehat{\tau})$ is the amplitude-dependent synchrotron frequency and $\hat{a}$ is a constant proportional to the squared amplitude of the betatron motion at the pick-up location. The argument of the Bessel function is given by

$$\chi^{\pm}_{\widehat{\tau}_i, n} = \left(n\widehat{\tau_i} \pm \frac{\widehat{Q_i}}{\Omega_{s_i}} \right) \omega_0 = (n\eta \pm Q\xi) \frac{\omega_0 \hat{p}}{\Omega_{s_i} p_0}, \quad (2)$$

with η denoting the slip factor and $\hat{p}$ the amplitude of momentum oscillations around the nominal value p_0. We assume that particles perform harmonic synchrotron motion, with the synchrotron frequency given by the theory of the mathematical pendulum [17]:

$$\Omega_s = \frac{\pi}{2\mathscr{K}\left[\sin\left(\frac{h_{RF}\omega_0\widehat{\tau}}{2}\right)\right]} \Omega_{s_0}, \quad (3)$$

where Ω_{s_0} is the nominal, limit synchrotron frequency, $h_{RF}\omega_0\widehat{\tau}$ is the the RF phase amplitude of synchrotron oscillations and $\mathscr{K}([0,1]) \to [\pi/2, \infty]$ denotes the complete elliptic integral of the first kind [18, p. 590].

In the absence of coherent components which, in the case of the transverse Schottky spectrum is equivalent to having a uniform distribution of both betatron and synchrotron oscillation phases, the total multiparticle PSD is given simply

ISBN: 978-3-95450-236-3 ISSN: 2673-5350 doi:10.18429/JACoW-IBIC2023-TH2C03

by the sum of individual PSDs

$$P_T^{\pm}(\omega, \Omega_{s_0}, Q, Q\xi) = \sum_{i=1}^{N} P_T^{\pm}(\omega, \widehat{\tau_i}, \Omega_{s_0}, Q, Q\xi). \quad (4)$$

As we can see, given a set of parameters Ω_{s_0}, Q and $Q\xi$, the Schottky spectrum can be fully determined by the distribution of synchrotron amplitudes $\widehat{\tau_i}$ within a given bunch. In [15] we also showed that, in the absence of coherent motion, one can also use the longitudinal bunch profile or the distribution of synchrotron frequencies to determine the distribution of synchrotron amplitudes.

An example theoretical transverse Schottky spectrum is shown in Fig. 1. Two sidebands, located around the frequencies $(h \pm Q_F)\omega_0$, consist of a series of *Bessel satellites*. The distance between consecutive satellites is given by the synchrotron frequency. Individual satellites have a finite width, which reflects the spread in synchrotron frequencies among the particles. For non-zero chromaticity, the upper (right) and lower (left) sidebands are different, what is a result of a different argument of the Bessel functions, Eq. (2).

One has to keep in mind, that the observed Schottky signal is an intrinsically random process and in each time instance one can observe only its single realization [19]. Meanwhile the theory presented here describes the expected value, i.e. the ensemble average, of the spectrum.

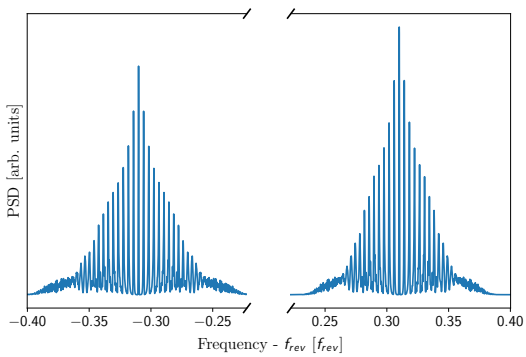

Figure 1: Theoretical transverse Schottky spectrum.

Assuming a discrete macroscopic distribution of synchrotron amplitudes $g(\widehat{\tau}_i)$ for an apriori chosen grid of synchrotron amplitudes $\widehat{\tau}_1, \ldots, \widehat{\tau}_m$, the DFT (Discrete Fourier Transform) of the total transverse Schottky signal at frequencies $\omega_1, \ldots, \omega_n$ can be expressed in a form of a matrix equation (Eq. (5)), where single particle $P_{DFT}^{T,\pm}$s can be calculated directly from Eq. (1), taking into the account the sampling frequency, period and the windowing function. The vector $\mathscr{A}$ denotes the discrete synchrotron amplitude distribution, while $\mathscr{S}_{DFT}$ is the DFT of the total Schottky signal. The number of considered amplitudes $\widehat{\tau_1}, \ldots, \widehat{\tau_n}$ has to be chosen as a trade-off between the time-complexity and discretisation error. In our studies we have used 50 amplitudes uniformly distributed over the whole RF bucket.

SCHOTTKY SIGNALS IN THE LHC

The LHC Schottky Monitor consists of four pairs of approximately 1 m waveguides, one for each of the 2 beams and the 2 planes, sensitive to the beam field within a band of approximately 400 MHz around 4.8 GHz. An electronic gating system allows one to isolate the signal coming from a single bunch. The coupled signal is then sequentially filtered and down-mixed, so that the final digitized Schottky signal consists of a narrow (approximately 14 kHz wide) band, originally located around the 427725^{th} harmonic of the revolution frequency, but mixed down to the 1^{st} harmonic.

The sampling rate, locked to the RF frequency to avoid discrepancies during the energy ramp, is kept equal to $4\times f_{rev}$. The spectra are calculated every second using the last $2^{16} = 65536$ samples, which results in a frequency resolution of approximately 0.69 Hz, and the expected value of the spectrum is estimated by performing a moving average of the last 100 spectra on a bin-by-bin basis.

The typical Schottky spectrum measured by the LHC Schottky monitor, in the absence of any coherent effects, consists of three bands: two transverse bands described by Eq. (4) plus the central longitudinal band. Although by design the strong longitudinal signal should not be seen by the monitor, imperfections of the common mode rejection make this signal visible and available for the diagnostic purposes, as discussed in Ref. [15].

The particle species accelerated in the LHC are either protons or Pb^{82+} ions. For the purpose of Schottky signals analysis, ion beams are significantly more favorable. Ion bunches consist of a lower number of particles, but each having a higher individual charge, they are therefore less likely to produce coherent effects in the spectrum. In addition, the higher transverse emittance of ion bunches increases the measured dipole moment, and therefore intensifies the transverse Schottky signal.

In Fig. 2 one can observe spectrograms and averaged spectra during typical stages of the ion beam operation. For ilustrative purposes only the upper transverse sideband is shown.

Figure 2 a) presents an unperturbed spectrum during steady conditions. Such a spectrum reliably reflect the theory discussed in the previous section, and can be easily analyzed. Spectra in Fig. 2 b) and c) were measured under conditions which introduced a local deformation of the averaged spectrum. The majority of the spectrum is however not affected, and can be matched with the theoretical description. The spectrogram shown in Fig. 2 d) is an example of a variety of transient effects, including different types of beam beam parameters change. Inevitably under these non-stationary conditions, and while the spectrogram is understandable, information is lost in the averaging process and the time averaged spectrum becomes very complex to analyse. Finally, Fig. 2 e) shows the spectrogram and average Schottky spectrum measured while the current in the octupole magnets is being ramped up. In this case individual Bessel satellites smear into wider bands (and eventually disappear for

ISBN: 978-3-95450-236-3 ISSN: 2673-5350 doi:10.18429/JACoW-IBIC2023-TH2C03

$$\underbrace{\begin{bmatrix} P^{T,\pm}_{DFT}(\omega_1,\widehat{\tau_1},\Omega_{s_0},Q,Q\xi) & \cdots & P^{T,\pm}_{DFT}(\omega_1,\widehat{\tau_n},\Omega_{s_0},Q,Q\xi) \\ P^{T,\pm}_{DFT}(\omega_2,\widehat{\tau_1},\Omega_{s_0},Q,Q\xi) & \cdots & P^{T,\pm}_{DFT}(\omega_2,\widehat{\tau_n},\Omega_{s_0},Q,Q\xi) \\ \vdots & \ddots & \vdots \\ P^{T,\pm}_{DFT}(\omega_m,\widehat{\tau_1},\Omega_{s_0},Q,Q\xi) & \cdots & P^{T,\pm}_{DFT}(\omega_m,\widehat{\tau_n},\Omega_{s_0},Q,Q\xi) \end{bmatrix}}_{\mathscr{M}(\Omega_{s_0},Q,Q\xi))} \cdot \underbrace{\begin{bmatrix} \tilde{g}(\widehat{\tau_1}) \\ \tilde{g}(\widehat{\tau_2}) \\ \vdots \\ \tilde{g}(\widehat{\tau_n}) \end{bmatrix}}_{\mathscr{A}} = \underbrace{\begin{bmatrix} P^{T,\pm}_{DFT}(\omega_1) \\ P^{T,\pm}_{DFT}(\omega_2) \\ \vdots \\ P^{T,\pm}_{DFT}(\omega_m) \end{bmatrix}}_{\mathscr{S}_{DFT}}, \tag{5}$$

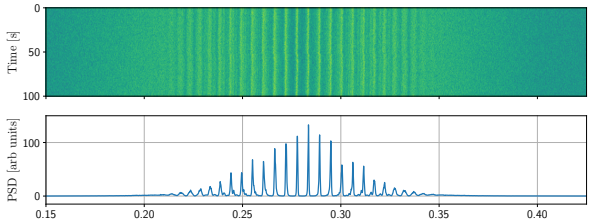

(a) Stable conditions

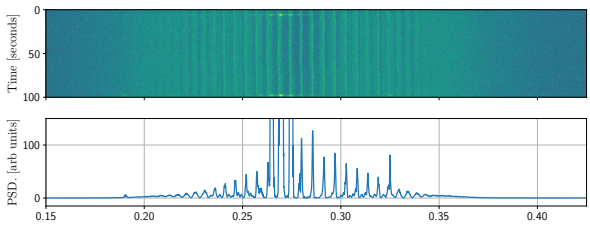

(b) Coupling measurement

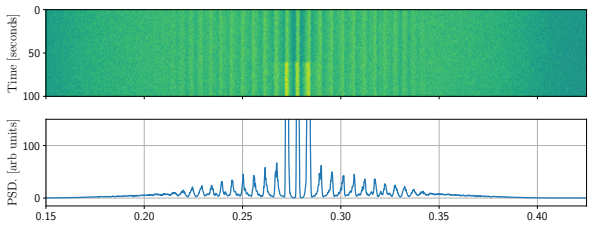

(c) Collimator movement

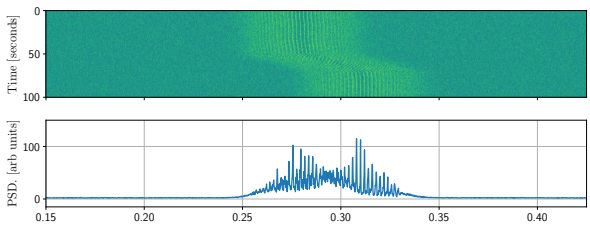

(d) Tune shift

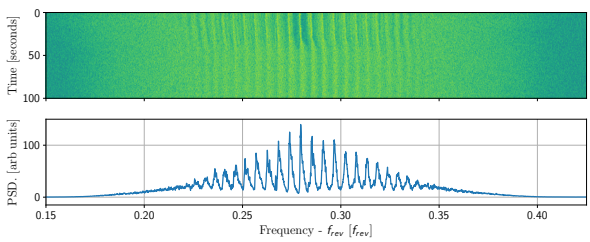

(e) Octupole ramp

Figure 2: Examples of upper sidebands of Schottky spectrograms and averaged spectra of ion beam. All, apart from (d), measured at the injection energy.

high enough octupole strength), corresponding to the tune spread induced by the octupoles. The authors of this contribution are not aware of any theoretical result explaining how transverse beam characteristics can be derived in such cases.

ANALYSIS

Of the various parameters that can be estimated from transverse Schottky spectra, some of the most important include the fractional betatron tune Q_F and the chromaticity $Q\xi$. Examining Eq. (1), one sees that the transverse sidebands are symmetric with respect to the frequencies $(h \pm Q_F)\omega_0$. The frequency bin corresponding to the tune value can then be determined as the one which minimizes the following expression:

$$C_{MD}(k) = \sum_{i=1}^{i=N} \left| P^{\pm}_T(\omega_{k-i}) - P^{\pm}_T(\omega_{k+i}) \right|. \tag{6}$$

If a higher tune resolution is desired, values in between the frequency bins can be interpolated.

In order to estimate chromaticity, it can be proven [16] that, for LHC conditions and RMS widths of the lower and upper transverse sidebands equal to Δf_- and Δf_+ respectively, the chromacity is given by

$$Q\xi = -\eta \left(n \frac{\Delta f_- - \Delta f_+}{\Delta f_- + \Delta f_+} - Q_I \right). \tag{7}$$

Application of Eqs. (6) and (7) requires stationary beam conditions and negligible coherent effects. In the case of the LHC, this is mostly achievable during Pb^{82+} ion runs. In Fig. 3 one can see the tune and chromaticity at flattop during LHC fill 8413, estimated using these formulas. The effect of octupole magnets is neglected here, what couldn't be done at injection energy due to the lower magnetic rigidity and higher transverse size of the beam. The resolution of the measured chromaticity is below the 3 units, the value required at flattop energy by the LHC design report [20].

During less favorable conditions, when spurious components are present in the spectrum as in Fig. 2 b) and c), a different approach has to be taken. A key observation is that Eq. (5) remains valid after removing an arbitrary number of rows from both matrix $\mathscr{M}$ and vector $\mathscr{S}_{DFT}$. If an unwanted component is present at frequency bins $\omega_i, \ldots, \omega_j$, these can be simply excluded from Eq. (5) forming new matrix $\tilde{\mathscr{M}}$ and vector $\tilde{\mathscr{S}}_{DFT}$. Then, the values of Q and $Q\xi$ can be obtained by minimizing the cost function:

$$C_T(\Omega_{s_0},\mathscr{A},Q,Q\xi) = |\tilde{\mathscr{M}}(\Omega_{s_0},Q,Q\xi)\cdot\mathscr{A} - \tilde{\mathscr{S}}_{exp}|^2, \tag{8}$$

ISBN: 978-3-95450-236-3 ISSN: 2673-5350 doi:10.18429/JACoW-IBIC2023-TH2C03

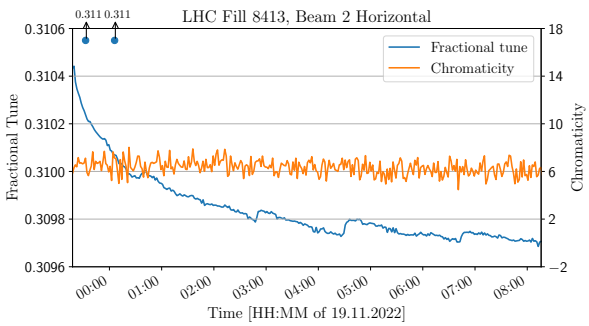

Figure 3: Q and $Q\xi$, estimated in stable beam conditions using Eqs. (6) and (7). Two tune outliers marked with dots.

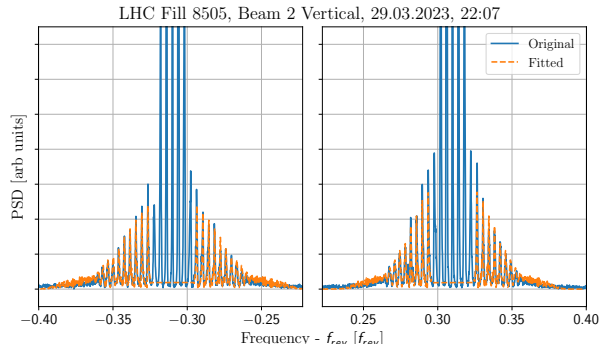

Figure 4: Measured and fitted transverse sidebands. The central part of each sideband was excluded from the analysis.

where $\mathscr{S}_{exp}$ is the experimentally measured Schottky spectrum and $|\cdot|$ denotes the standard Euclidean norm. Similarly, the betatron tune can also be obtained by modifying Eq. (6) in a way where only frequency bins which do not contain coherent components are included in the sum, and the results is then scaled by the number of elements in the sum.

In addition, it is also possible to estimate Ω_{s_0} and $\mathscr{A}$, apriori, either from the longitudinal part of the spectrum as shown in [15], or by measuring using other instruments. At the LHC, the synchrotron amplitude distributions can be calculated from measured longitudinal bunch profiles [15, 21], while the nominal synchrotron frequency is possible to derive either from the peak detected Schottky system [22] or calculated based on the knowledge of the voltage in the RF cavities. The cost function given by Eq. (8) can be minimized using optimization routines, such as L-BFGS-B [23] or differential evolution algorithms [24]. Both approaches have been successfully used in Refs. [15, 16]. This approach has been used on transverse proton spectra acquired shortly after the restart of the LHC in 2023 (fill 8505), at injection energy. As can be seen in Fig. 4, the central satellites are significantly enhanced, which suggests the presence of residual coherence in the particles' synchro-betatron motion. To eliminate their impact on the analysis, the central frequency bins have been excluded. The betatron tune was calculated using Eq. (6), modified as explained previously, while the nominal synchrotron frequency was determined based on the RF voltage and corrected using the Schottky spectra in an independent analysis of the longitudinal part of the spectrum. The minimization of Eq. (8), using the differential evolution algorithm from SciPy library, required finding only three distinct parameters, under the assumption that $\mathscr{A}$ follows the Rice distribution [25]. The obtained fit, that is $\tilde{\mathscr{M}} \cdot \mathscr{A}$ for optimal parameters, is compared with the experimental spectrum in Fig. 4, while estimated values of the betatron tune and chromaticity are presented in Fig. 5. As a reference for comparison, both the chromaticity estimated with the invasive RF-modulation technique [26] is shown as the dashed black line, as well as the chromaticity calculated using Eq. (7).

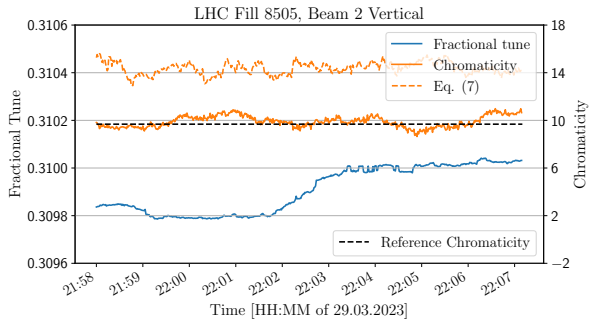

Figure 5: Q and $Q\xi$, estimated in the presence of coherent components, using modifed Eq. (6) and spectra fitting.

CONCLUSION

In this contribution we presented results and discussed some of the challenges associated with the analysis of the Schottky spectra at the LHC. We have demonstrated how a new fitting technique can help to overcome problems with the analysis of spectra containing strong localized components.

The online implementation of the Schottky spectrum analysis is in the final stage of development and is planned to be validated during the LHC ion campaing during the fall of 2023. In parallel, studies are ongoing in order to better understand the spectra, for example including the effect of octupole magnets and beam coupling impedance [27].

The future steps towards further understanding of Schottky spectra and improvement of the beam diagnostic procedures should focus on the developing the theory of Schottky signals which includes the effect of octupole magnets. Very beneficial would also be to investigate the possibilities of using image recognition techniques to analyze 2D Schottky spectrograms.

REFERENCES

[1] J. Borer *et al.*, "Non-destructive diagnostics of coasting beams with Schottky noise", in *Proc. 9th International Conference on High-energy Accelerators*, Stanford, CA, USA, May 1974, pp. 53–56.

[2] S. van der Meer, "Stochastic damping of betatron oscillations in the ISR", CERN, Geneva, Switzerland, Rep. CERN-ISR-

ISBN: 978-3-95450-236-3 ISSN: 2673-5350 doi:10.18429/JACoW-IBIC2023-TH2C03

PO-72-31, 1972.

[3] A. Jansson, P. Lebrun, and R. Pasquinelli, "Experience with the 1.7 GHz Schottky Pick-ups in the Tevatron", in *Proc. EPAC'04*, Lucerne, Switzerland, Jul. 2004, paper THPLT135, pp. 2777–2779.

[4] A. Sukhanov, K. A. Brown, C. W. Dawson, J. P. Jamilkowski, A. Marusic, and J. Morris, "Processing of the Schottky Signals at RHIC", in *Proc. ICALEPCS'17*, Barcelona, Spain, Oct. 2017, pp. 1327–1329. doi:10.18429/JACoW-ICALEPCS2017-THMPA08

[5] R. Singh *et al.*, "Interpretation of transverse tune spectra in a heavy-ion synchrotron at high intensities", *Phys. Rev. ST Accel. Beams*, vol. 16, no. 3, pp. 034201, 2013. doi:10.1103/PhysRevSTAB.16.034201

[6] Wu, J. *et al.*, "Performance of the resonant Schottky pickup at CSRe", *Nucl. Instrum. Methods Phys. Res., Sect. B*, vol. 317, pp. 623–628, 2013. doi:10.1016/j.nimb.2013.08.017

[7] L. Soby *et al.*, "Elena Orbit and Schottky Measurement Systems", in *Proc. IPAC'15*, Richmond, VA, USA, May 2015, pp. 1061–1064. doi:10.18429/JACoW-IPAC2015-MOPTY056

[8] M. Betz *et al.*, "Bunched-beam Schottky monitoring in the LHC", *Nucl. Instrum. Methods Phys. Res., Sect. A*, vol. 874, pp. 113–126, 2017. doi:10.1016/j.nima.2017.08.045

[9] S. van der Meer, "Diagnostics with Schottky noise", in *Proc. 3rd Joint US-CERN School on Particle Accelerators*, Anacapri, Italy, Oct. 1988, pp. 423-433.

[10] S. Paret *et al.*, "Transverse Schottky and beam transfer function measurements in space charge affected coasting ion beams", *Phys. Rev. ST Accel. Beams*, vol. 13, no. 2, pp. 022802, 2010. doi:10.1103/PhysRevSTAB.13.022802

[11] L. J. Mao *et al.*, "A Characteristics Study for Cold Ion Beam Momentum Spread at HIRFL-CSR", in *Proc. IPAC'10*, Kyoto, Japan, May 2010, paper TUPD012, pp. 1946–1948.

[12] D. Boussard, "Schottky noise and beam transfer function diagnostics," in *Proc. CERN Accelerator School: Advanced Accelerator Physics course*, pp.749-782, 1995. doi:10.5170/CERN-1995-006.749

[13] S. Chattopadhyay, "Some fundamental aspects of fluctuations and coherence in charged-particle beams in storage rings", CERN, Geneva, Switzerland, 1984. doi:10.5170/CERN-1984-011

[14] O. Boine-Frankenheim and V. Kornilov, "Transverse Schottky noise spectrum for bunches with space charge". *Phys. Rev. ST Accel. Beams*, vol. 12, no. 11, pp. 114201, 2009. doi:10.1103/PhysRevSTAB.12.114201

[15] K. Lasocha and D. Alves, "Estimation of longitudinal bunch characteristics in the LHC using Schottky-based diagnostics", *Phys. Rev. Accel. Beams*, vol. 23, no. 6, pp. 062803, 2020. doi:10.1103/PhysRevAccelBeams.23.062803

[16] K. Lasocha and D. Alves, "Estimation of transverse bunch characteristics in the LHC using Schottky-based diagnostics", *Phys. Rev. Accel. Beams*, vol. 25, no. 6, pp. 062801, 2022. doi:10.1103/PhysRevAccelBeams.25.062801

[17] K. Ochs, "A comprehensive analytical solution of the nonlinear pendulum", *Eur. J. Phys.*, vol. 32, no. 2, p. 479, 2011. doi:10.1088/0143-0807/32/2/019

[18] M. Abramowitz and I. A. Stegun, *Handbook of Mathematical Functions with Formulas, Graphs, and Mathematical Tables*, 9th ed, Dover, 1964. doi:10.1119/1.15378

[19] C. Lannoy *et al.* "Statistical Properties of Schottky Spectra", in *Proc. IBIC'23*, Saskatoon, Canada, Sep. 2023, paper WEP035, this conference.

[20] O. S. Brüning *et al.*, *LHC Design Report*, CERN Yellow Reports: Monographs, CERN, Geneva, Switzerland, 2004. doi:10.5170/CERN-2004-003-V-1

[21] J. Jõul, "Software development for a high-speed digitizer to provide online access to longitudinal bunch profiles in the Large Hadron Collider", Master Thesis, Tartu University, 2023.

[22] E. N. Shaposhnikova, T. Bohl, and T. P. R. Linnecar, "Longitudinal Peak Detected Schottky Spectrum", in *Proc. HB'10*, Morschach, Switzerland, Sep.-Oct. 2010, paper TUO1C04, pp. 363–367.

[23] R. Byrd *et al.*, "A limited memory algorithm for bound constrained optimization", *SIAM J. Sci. Comput.*, vol. 16, no. 5, pp. 1190-1208, 1995. doi:10.1137/0916069

[24] R. Storn and K. Price, "Differential evolution - a simple and efficient heuristic for global optimization over continuous spaces", *J. Global Optim.*, vol. 11, pp. 341–-359, 1997. doi:10.1023/A:1008202821328

[25] A. Abdi *et al.*, "On the estimation of the K parameter for the Rice fading distribution", *IEEE Commun. Lett.*, vol. 5, no. 3, pp. 92–94, 2001. doi:10.1109/4234.913150

[26] O. S. Brüning , W. Höfle, R. Jones, T. Linnecar, and H. Schmickler, "Chromaticity Measurements via RF Phase Modulation and Continuous Tune Tracking", in *Proc. EPAC'02*, Paris, France, Jun. 2002, paper THPRI061, pp. 1852–1854.

[27] C. Lannoy *et al.* "Effect of Longitudinal Beam-Coupling Impedance on the Schottky Spectrum of Bunched Beams", in *Proc. IBIC'23*, Saskatoon, Canada, Sep. 2023, paper WEP034, this conference.